Simple Stochastic Dynamical Models Capturing the Statistical Diversity of El Niño Southern Oscillation (Supporting Information Appendix)

Nan Chen and Andrew J. Majda

Department of Mathematics, and Center for Atmosphere Ocean Science, Courant Institute of Mathematical Sciences, New York University, 251 Mercer Street, New York, NY 10012 USA

This *SI Appendix* consists of three sections. Section 1 involves a brief model derivations and the low-order meridional truncation. The parameter values in the coupled model and the mathematical formulae of the anomalous Walker circulation are also included in this section. Section 2 contains the details of determining the transition rates in the three-state Markov jump process according to the observations. Section 3 includes sensitivity test.

1 Model derivations, meridional truncation and parameter choices

The coupled model considered in this article is derived from a more complicated model that consists of the skeleton model in the atmosphere [1, 2] coupled to a shallow water ocean in the long-wave approximation and a sea surface temperature (SST) budget [3]. Then an asymptotic expansion with respect to a small factor ϵ that is the ratio of intraseasonal time scale over the interannual one is applied and the result is Eq. (1)-(4) in the article. The details of model derivation are contained in the *SI Appendix* of [4]. For the convenience of statement, we summarize the coupled model below.

1. Atmosphere model:

$$\begin{aligned} &-yv-\partial_x\theta=0,\\ &yu-\partial_y\theta=0,\\ &-(\partial_x u+\partial_y v)=E_q/(1-\bar{Q}). \end{aligned} \tag{1.1}$$

2. Ocean model:

$$\begin{aligned} &\partial_\tau U-c_1YV+c_1\partial_x H=c_1\tau_x,\\ &YU+\partial_Y H=0,\\ &\partial_\tau H+c_1(\partial_x U+\partial_Y V)=0. \end{aligned} \tag{1.2}$$

3. SST model:

$$\partial_\tau T+\mu\partial_x\big(UT\big)=-c_1\zeta E_q+c_1\eta H. \tag{1.3}$$

1.1 Meridional truncation

In order to compute the solutions of the coupled model, we consider the model in its simplest form, which is truncated meridionally to the first parabolic cylinder functions [6].

Different parabolic cylinder functions are utilized in the ocean and atmosphere due to the difference in their deformation radii. The first atmospheric parabolic cylinder function reads $\phi_0(y) = (\pi)^{-1/4}\exp(-y^2/2)$, and the third one that will be utilized as the reconstruction of solutions reads $\phi_2 = (4\pi)^{-1/4}(2y^2-1)\exp(-y^2/2)$. The oceanic parabolic cylinder functions read $\psi_m(Y)$, which are identical to the expressions of the atmospheric ones except depending on the Y axis.

In the atmosphere we assume a truncation of moisture, wave activity and external sources to the first parabolic cylinder function ϕ_0. This is known to excite only the Kelvin and first Rossby atmospheric equatorial waves, of amplitude K_A and R_A [1, 2]. In the ocean, we assume a truncation of zonal wind stress forcing to ψ_0, $\tau_x = \tau_x\psi_0$. This is known to excite only the the Kelvin and first Rossby atmospheric oceanic waves, of amplitude K_O and R_O. Similarly, for the SST model we assume a truncation ψ_0, $T = T\psi_0$. The ENSO model truncated meridionally reads:

1. Atmosphere model:

$$\begin{aligned} &\partial_x K_A = \chi_A(E_q - \langle E_q\rangle)(2-2\bar{Q})^{-1},\\ &-\partial_x R_A/3 = \chi_A(E_q - \langle E_q\rangle)(3-3\bar{Q})^{-1}, \end{aligned} \tag{1.4}$$

2. Ocean model:

$$\begin{aligned} &\partial_\tau K_O + c_1\partial_x K_O = \chi_O c_1\tau_x/2,\\ &\partial_\tau R_O - (c_1/3)\partial_x R_O = -\chi_O c_1\tau_x/3, \end{aligned} \tag{1.5}$$

3. SST model:

$$\partial_\tau T + \mu\partial_x\big((K_O - R_O)T\big) = -c_1\zeta E_q + c_1\eta H, \tag{1.6}$$

where χ_A and χ_O are the projection coefficients from ocean to atmosphere and from atmosphere to ocean, respectively, due to the different extents in their meridional bases. The latent heating is linearized with $E_q = \alpha_q T$ in the Pacific band and zero outside. Due to the absence of dissipation in the atmosphere, the solvability condition requires a zero equatorial zonal mean of latent heating forcing $\langle E_q\rangle$ [7, 8]. Note that when meridional truncation is implemented, a projection coefficient $\chi \approx 0.65$ appears in front of the nonlinear term [2], which here is absorbed into the nonlinear advection coefficient μ for the notation simplicity and the parameter μ in the Table below has already taken into account this projection coefficient.

Now instead of solving the coupled system (1.1)–(1.3), we solve the system (1.4)–(1.6). Periodic boundary conditions are adopted for the atmosphere model (1.4). Reflection boundary conditions are adopted for the ocean model (1.5),

$$K_O(0,t) = r_W R_O(0,t), \qquad R_O(L_O,t) = r_E K_O(L_O,t), \tag{1.7}$$

where $r_W = 0.5$ representing partial loss of energy in the west Pacific boundary across Indonesian and Philippine and $r_E = 0.5$ representing partial loss of energy due to the north-south propagation of the coast Kelvin waves along the eastern Pacific boundary. Note that r_E here is different from the one taken in [4] ($r_E = 1$), where a perfect reflection is assumed. For the SST model, no normal derivative at the boundary of T is adopted, i.e. $dT/dx = 0$.

To prevent nonphysical boundary layers in the finite difference method, the coupled model is solved through an upwind scheme, where some details of discretization is included in the *SI Appendix* of [4, 5]. The total grid points in the ocean and in the atmosphere are $N_O = 56$ and $N_A = 128$, respectively, which are doubled compared with that in [4] for the purpose of resolving some small scale interactions due to the nonlinearity. The time step is $\Delta t = 4.25$ hours. The ratio $\Delta t/\Delta x$ is approximately 0.115 under the nondimensional values.

The physical variables can be easily reconstructed in the following way.

$$\begin{aligned} u &= (K_A - R_A)\phi_0 + (R_A/\sqrt{2})\phi_2, \\ \theta &= -(K_A + R_A)\phi_0 - (R_A/\sqrt{2})\phi_2, \\ v &= (4\partial_x R_A - \bar{H}A - S^\theta)(3\sqrt{2})^{-1}\phi_1, \\ U &= (K_O - R_O)\psi_0 + (R_O/\sqrt{2})\psi_2, \\ H &= (K_O + R_O)\psi_0 + (R_O/\sqrt{2})\psi_2. \end{aligned} \tag{1.8}$$

See [2, 4, 5] for more details. The variables in (1.8) are utilized in showing the Hovmoller diagrams in Figure 4 and 5 of the main article.

1.2 Choices of parameters values

Two tables are included below. Table 1 summarizes the variables in the coupled model and lists the associated units and the typical unit values. Table 2 shows the nondimensional values of the parameters that are utilized in the meridional truncated model (1.4)–(1.6).

Variable	unit	unit value
x zonal axis	$[y]/\delta$	$15000km$
y meridional axis atmosphere	$\sqrt{c_A/\beta}$	$1500km$
Y meridional axis ocean	$\sqrt{c_O/\beta}$	$330km$
t time axis intraseasonal	$1/\delta\sqrt{c_A\beta}$	$3.3\,days$
τ time axis interannual	$[t]/\epsilon$	$33\,days$
u zonal wind speed anomalies	δc_A	$5\,ms^{-1}$
v meridional wind speed anomalies	$\delta[u]$	$0.5\,ms^{-1}$
θ potential temperature anomalies	15δ	$1.5K$
q low-level moisture anomalies	$[\theta]$	$1.5K$
a envelope of synoptic convective activity	1	
$\overline{H}a$ convective heating/drying	$[\theta]/[t]$	$0.45\,K.day^{-1}$
E_q latent heating anomalies	$[\theta]/[t]$	$0.45\,K.day^{-1}$
T sea surface temperature anomalies	$[\theta]$	$1.5K$
U zonal current speed anomalies	$c_O\delta_O$	$0.25\,ms^{-1}$
V zonal current speed anomalies	$\delta\sqrt{c}[U]$	$0.56\,cms^{-1}$
H thermocline depth anomalies	$H_O\delta_O$	$20.8\,m$
τ_x zonal wind stress anomalies	$\delta\sqrt{\beta/c_A}\,H_O\rho_O c_O^2\delta_O$	$0.00879\,N.m^{-2}$
τ_y meridional wind stress anomalies	$[\tau_x]$	$0.00879\,N.m^{-2}$

Table 1: Definitions of model variables and units in the meridional truncated model.

Parameter	description	Nondimensional values
c	ratio of ocean and atmosphere phase speed	0.05
ϵ	Froude number	0.1
c_1	ratio of c/ϵ	0.5
χ_A	Meridional projection coefficient from ocean to atmosphere	0.32
χ_O	Meridional projection coefficient from atmosphere to ocean	1.30
L_A	Equatorial belt length	8/3
L_O	Equatorial Pacific length	1.16
γ	wind stress coefficient	6.529
r_W	Western boundary reflection coefficient in ocean	0.5
r_E	Eastern boundary reflection coefficient in ocean	0.5
ζ	Latent heating exchange coefficient	8.5
α_q	Latent heating factor	0.3782
$\bar{Q}$	mean vertical moisture gradient	0.9
μ	nonlinear zonal advection coefficient	0.08
d_p	dissipation coefficient in the wind burst model	3.4

Table 2: Nondimensional values of the parameters.

1.3 Anomalous Walker circulation

In the atmospheric model (see [1] for the original version of the skeleton model), only the first baroclinic mode is included in the vertical direction, which has a profile of $\cos(z)$ function. Also recall that the coupled model is projected to the leading parabolic cylinder function in the meridional direction, which has a Gaussian profile that centers at the equator. Thus, the meridional derivative at the equator is $\partial_y \phi_0(y) = 0$ and the mass conservation equation reduces to

$$\tilde{u}_x(x,z) + \tilde{w}_z(x,z) = 0, \tag{1.9}$$

where $\tilde{u}(x,z)$ and $\tilde{w}(x,z)$ are the zonal and vertical velocities, respectively, which are functions of both x and z. Recall that the zonal velocity can be written as [1]

$$\tilde{u}(x,z) = u(x)\cos(z). \tag{1.10}$$

To satisfy the mass conservation condition (1.9), the vertical velocity is given by

$$\tilde{w}(x,z) = w(x)\cos(z) = -u_x(x)\sin(z), \tag{1.11}$$

where $w(x) = -u_x(x)$. In the dimensional form (variables with notation $\cdot^D$),

$$w^D(x) = -\frac{[H_v]}{[L]} u_x^D(x), \tag{1.12}$$

where $[H_v] = 16/\pi$km is the vertical length scale and $[L] = 15000$km is the horizonal length scale with nondimensional range $x \in [0, 1.17], z \in [0, \pi]$. The pair $\Big(\tilde{u}(x,z), \tilde{w}(x,z)\Big)$ forms the anomalous Walker circulation above the equatorial Pacific ocean as shown in Figure 4 of the main article.

2 Details of the transition rates in the three-state Markov jump process

Recall the governing equation of the stochastic wind burst amplitude a_p,

$$\frac{da_p}{d\tau} = -d_p(a_p - \hat{a}_p(T_W)) + \sigma_p(T_W)\dot{W}(\tau), \tag{2.1}$$

As discussed in the main article, a three-state Markov jump process is adopted for the parameters in (2.1),

$$\text{State 2:} \qquad \sigma_{p2} = 2.6, \qquad d_{p2} = 3.4, \qquad \hat{a}_{p2} = -0.25, \tag{2.2}$$

$$\text{State 1:} \qquad \sigma_{p1} = 0.8, \qquad d_{p1} = 3.4, \qquad \hat{a}_{p1} = -0.25, \tag{2.3}$$

$$\text{State 0:} \qquad \sigma_{p0} = 0.3, \qquad d_{p0} = 3.4, \qquad \hat{a}_{p0} = 0, \tag{2.4}$$

where State 2 corresponds to the traditional El Nino and State 1 to the CP El Nino while State 0 stands for quiescent phases. We assume all the three states can switch between each other. The detailed forms of the transition rates are shown below, which are functions of T_W, the averaged SST over the western Pacific. These transition rates are determined in accordance with the observational facts [13] as will be discussed below.

- The transition rates from State 2 to State 1 and from State 2 to State 0 are given by respectively

$$\nu_{21} = \frac{1}{10} \cdot \frac{1 - \tanh(2T_W)}{4}, \tag{2.5}$$

$$\nu_{20} = \frac{9}{10} \cdot \frac{1 - \tanh(2T_W)}{4}. \tag{2.6}$$

  Starting from State 2, the probability of switching to State 0 is much higher than that to State 1. This comes from the fact that a traditional El Niño is usually followed by a La Niña rather than a CP El Niño (e.g., year 1963, 1965, 1972, 1982 and 1998). Typically, the La Niña event has a weaker amplitude and a longer duration compared with the preceding El Niño. This actually corresponds to a discharge phase of the ENSO cycle with no external wind bursts (State 0).

- The transition rates from State 1 to State 0 and from State 1 to State 2 are given by respectively

$$\nu_{10} = \frac{1 - \tanh(2T_W)}{12}, \tag{2.7}$$

$$\nu_{12} = \frac{1 + \tanh(2T_W)}{40}, \tag{2.8}$$

  Although the denominator of ν_{10} is smaller than that of ν_{12}, quite a few CP El Niño events are associated with a slight positive T_W in the model, which means the transition rate ν_{12} is not necessarily smaller than ν_{10}. In fact, with the transition rates given by (2.7)–(2.8), the results show in the main article that more events are transited from state 1 to 2 than from state 1 to 0. This is consistent with the observations (e.g., year 1981 and 1995), implying that the CP El Niño is more likely to be followed by the classical El Niño than the quiescent phase.

- The transition rates from State 0 to State 1 and State 2 are given by

$$\nu_{01} = \frac{2}{3} \cdot \frac{1 + \tanh(2T_W)}{7}, \tag{2.9}$$

$$\nu_{02} = \frac{1}{3} \cdot \frac{1 + \tanh(2T_W)}{7}. \tag{2.10}$$

  Again, the transition rates to State 1 and 2 are different. This is due to the fact that after a quiescent period or discharge La Niña phase, more events are prone to becomes CP El Niño as a intermediate transition instead of directly forming another traditional El Niño (e.g., year 1969, 1977, 1990 and 2002).

Note that in (2.5)–(2.10), the transition rate ν_{ij} from a more active state to a less active state (with $i > j$) is always proportional to $1 - \tanh(2T_W)$ while that from a less active state to a more active state (with $i < j$) is always proportional to $1 + \tanh(2T_W)$. These are consistent with the fact stated in the main article that a transition from a less active to a more active state is more likely when $T_W \geq 0$ and vice versa.

3 Sensitivity test

With the optimal parameters of the transition rates shown in (2.5)–(2.10), the variance of the three T indices almost perfectly match those of the Nino indices and the non-Gaussian statistical characteristics in different Nino regions are recovered. Since most of the general circulation models tend to be sensitive to parameter perturbations [14, 15, 16], it is important to test the robustness of the coupled model studied in the main article. To this end, some perturbations are added to the transition rates and the statistics with the suboptimal rates are shown in the following. In each of the panel below, the variable with asterisk stands for the optimal value given by (2.5)–(2.10). The maximum perturbation of each transition rate is $\pm 25\%$.

In Figure S1–S3, the variance, skewness and kurtosis of T-3, T-3.4 and T-4 are shown as functions of perturbed transition rates. It is clear that all these statistics are fairly robust with respect to the parameter perturbations, where the variance of different T indices remain nearly the same as those in nature and the non-Gaussian features are still significant. The only parameter that is slightly sensitive is the transition rate from State 1 to State 2, i.e., ν_{12}. In fact, an underestimated ν_{12} modifies not only the frequency of both the CP and traditional El Niño but also the development of the nonlinear advective mode [5], which affect the PDFs in different Nino regions.

Other sensitivity tests with respect to the parameter perturbations in the coupled ocean-atmosphere were shown in the previous study [4]. The results there also indicate the robustness of the coupled model.

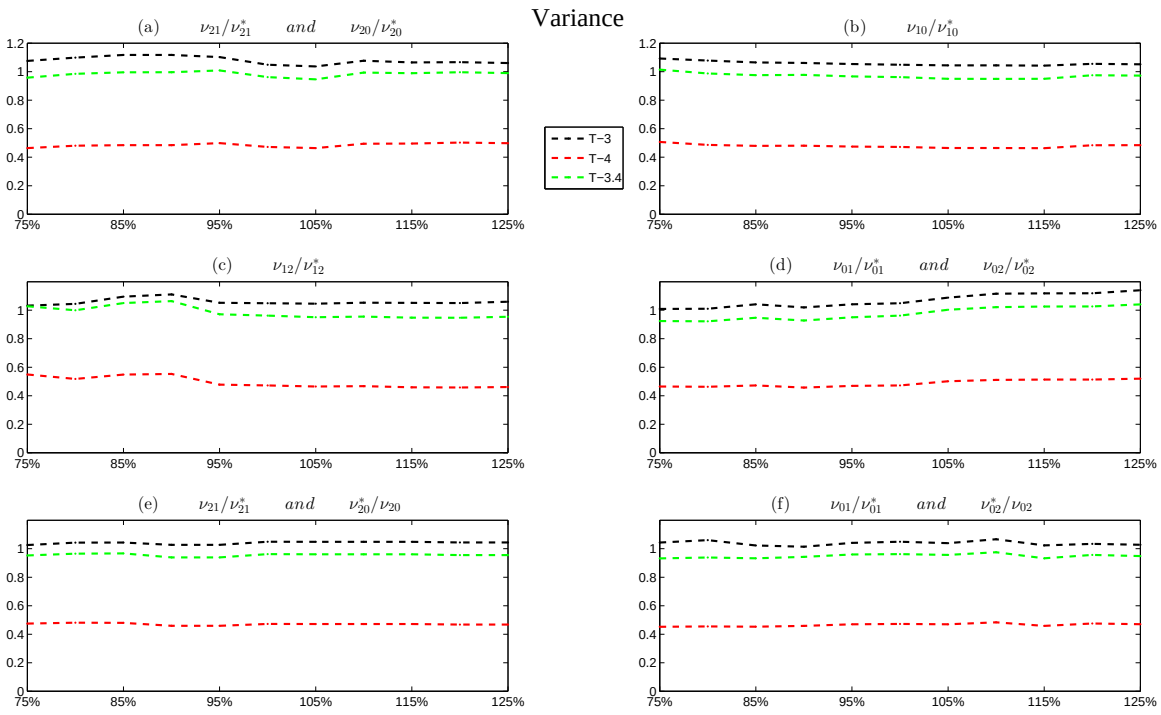

Figure S1: Sensitivity test. The variance of the three T indices as functions of suboptimal transition rates, where the variable with asterisk stands for the optimal value in (2.5)–(2.10).

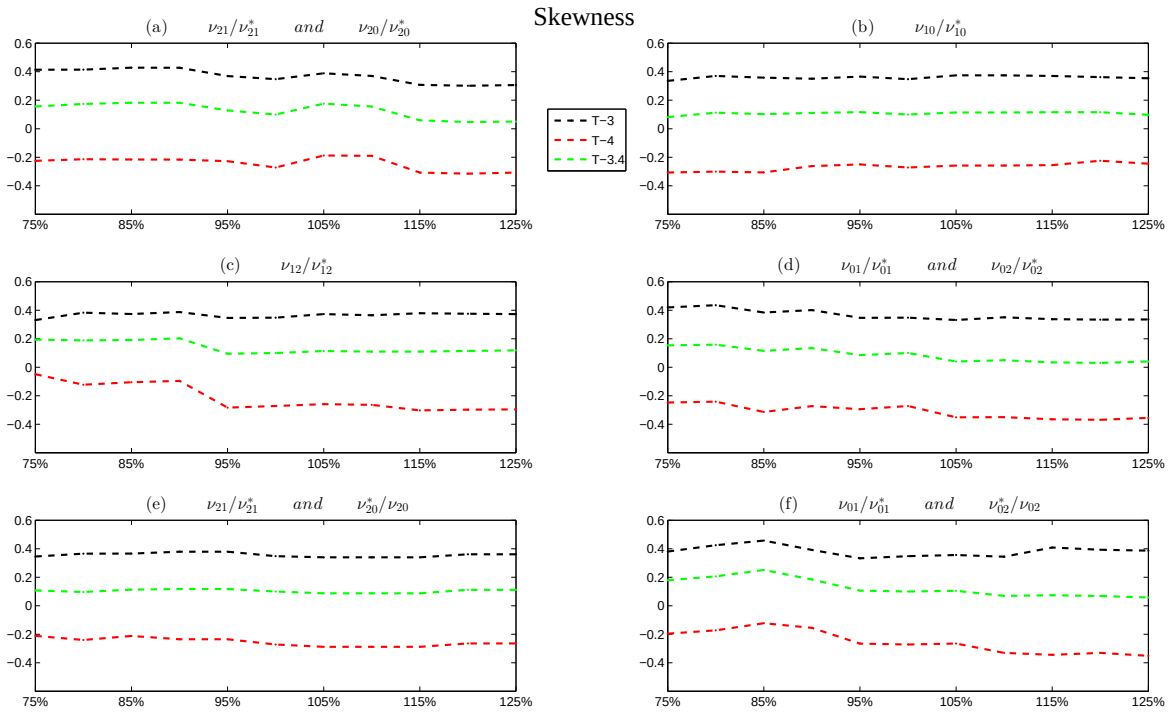

Figure S2: Sensitivity test. The skewness of the three T indices as functions of suboptimal transition rates, where the variable with asterisk stands for the optimal value in (2.5)–(2.10).

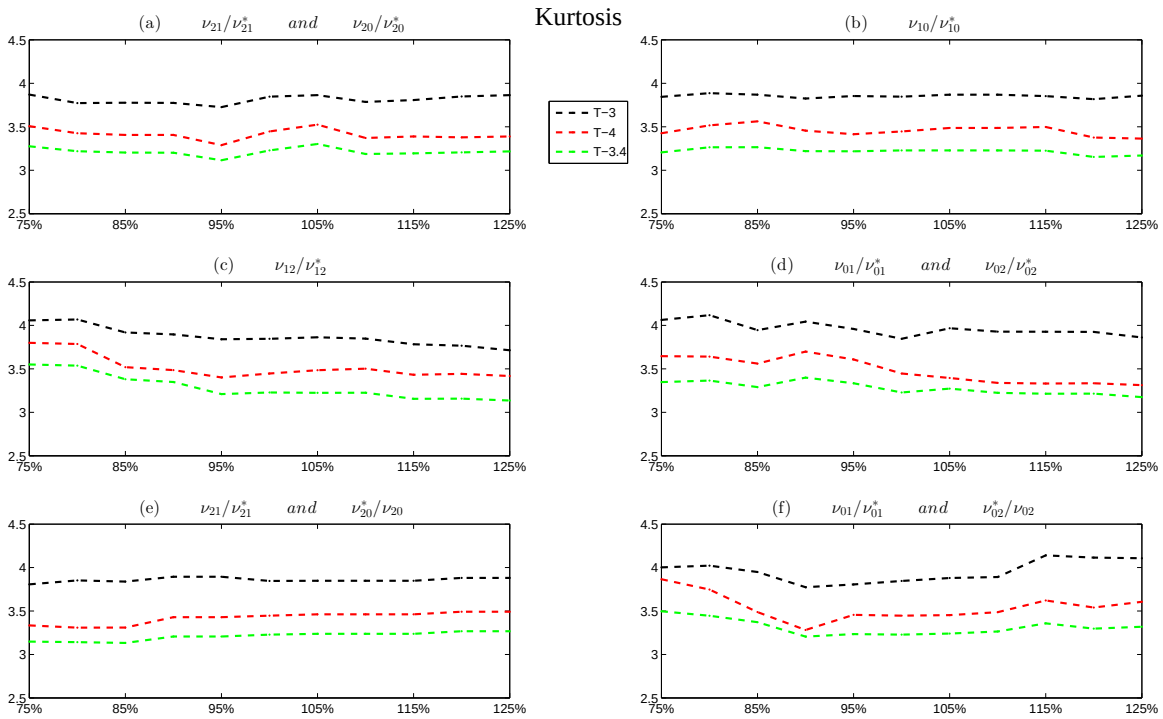

Figure S3: Sensitivity test. The kurtosis of the three T indices as functions of suboptimal transition rates, where the variable with asterisk stands for the optimal value in (2.5)–(2.10).

References

[1] Majda AJ, Stechmann SN (2009). The skeleton of tropical intraseasonal oscillations. *Proceedings of the National Academy of Sciences*, 106(21):8417-22.

[2] Majda AJ, Stechmann SN (2011). Nonlinear dynamics and regional variations in the MJO skeleton. *Journal of the Atmospheric Sciences*, 68(12):3053-71.

[3] Moore AM, Kleeman R (1999). Stochastic forcing of ENSO by the intraseasonal oscillation. *Journal of Climate*, 12(5):1199-1220.

[4] Thual S, Majda AJ, Chen N, Stechmann SN (2016). A simple stochastic model for El Niño with westly wind bursts. *Proceedings of the National Academy of Sciences*, 113(37):10245-10250, 2016.

[5] Chen N, Majda AJ, (2016). Simple dynamical models capturing the key features of the central Pacific El Niño. *Proceedings of the National Academy of Sciences*, 113(42):11732-11737.

[6] Majda A (2003). Introduction to PDEs and Waves for the Atmosphere and Ocean. *American Mathematical Soc.*

[7] Majda AJ, Klein R (2003). Systematic multiscale models for the tropics. *Journal of the Atmospheric Sciences*, 60(2):393-408.

[8] Stechmann SN, Ogrosky HR (2014). The Walker circulation, diabatic heating, and outgoing longwave radiation. *Geophysical Research Letters*, 41(24):9097-105.

[9] Majda AJ, Harlim J (2012). *Filtering complex turbulent systems.* (Cambridge University Press).

[10] Tziperman E, Yu L (2007). Quantifying the dependence of westerly wind bursts on the large-scale tropical Pacific SST. *Journal of climate*, 20(12):2760-8.

[11] Vecchi GA, Harrison DE (2000). Tropical Pacific Sea surface temperature anomalies, El Nino, and Equatorial Westerly Wind Events. *Journal of climate*, 13(11):1814-30.

[12] Hendon HH, Wheeler MC, Zhang C (2007). Seasonal dependence of the MJO-ENSO relationship. *Journal of Climate*, 20(3):531-43.

[13] Chen D, et al (2015). Strong influence of westerly wind bursts on El Niño diversity. *Nature Geoscience* 8(5): 339-345.

[14] Ham YG, Kug JS (2012). How well do current climate models simulate two types of El Niño? *Climate dynamics*, 39(1-2): 383-398.

[15] Kug JS, et al (2012). Improved simulation of two types of El Niño in CMIP5 models. *Environmental Research Letters*, 7(3): 034002.

[16] Ault TR, et al (2013). Characterizing decadal to centennial variability in the equatorial Pacific during the last millennium. *Geophysical Research Letters*, 40(13): 3450-3456.